*Graphical Abstract (for review)

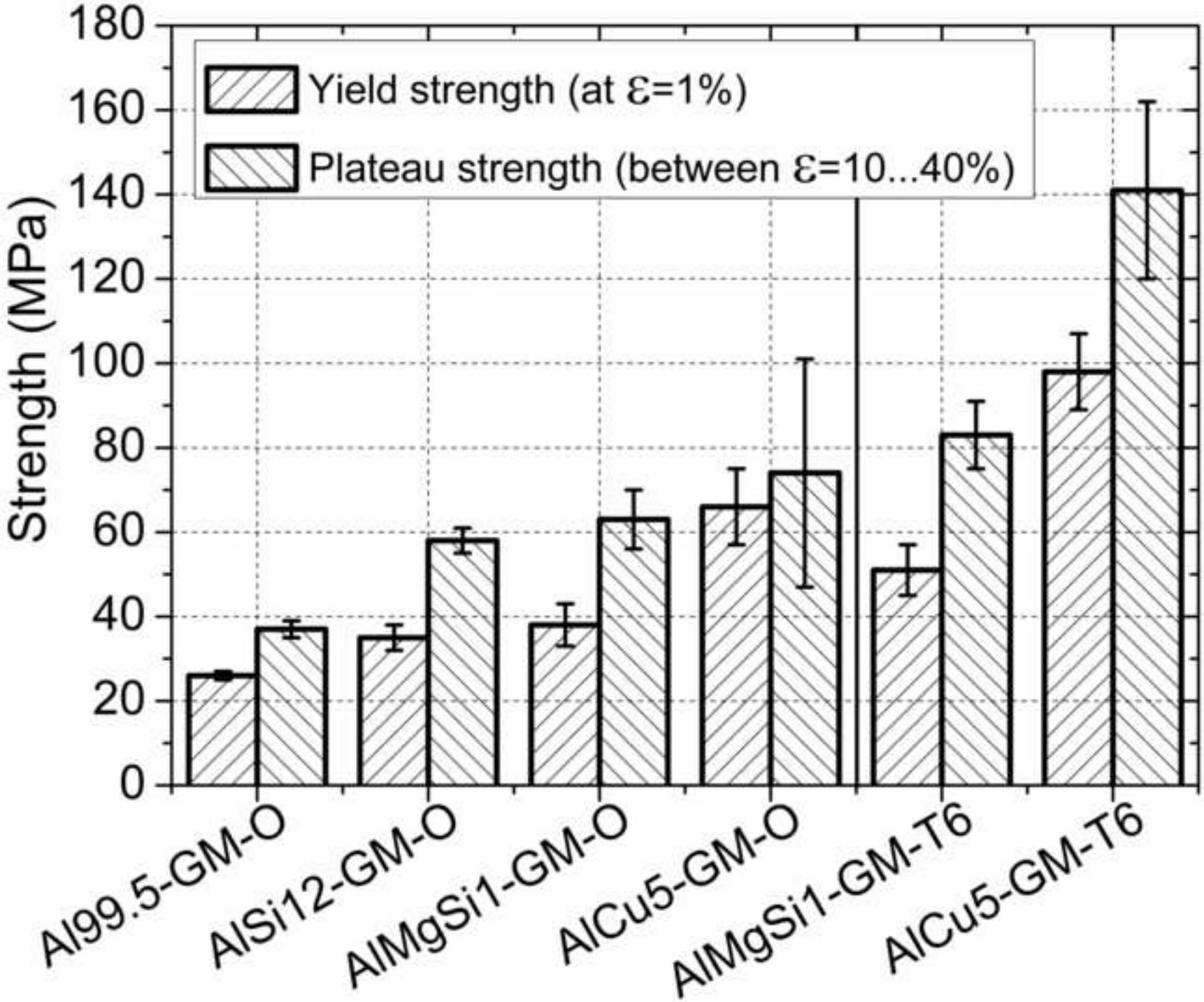

Highlights

- Low pressure infiltration is suitable to produce MMSFs with hollow iron spheres.
- The MMSFs showed plastic yielding and long, slowly ascending plateau region.
- The matrix and the heat treatment strongly influence the properties of the MMSFs.
- The full-scale FEM model gives excellent agreement compared to the measured values.

Compressive behaviour of aluminium matrix syntactic foams reinforced by iron hollow spheres

Attila SZLANCSIK[a], Bálint KATONA[a], Kristóf BOBOR[a], Kornél MÁJLINGER[a], Imre Norbert ORBULOV[a,b,*]

[a]Department of Materials Science and Engineering, Faculty of Mechanical Engineering, Budapest University of Technology and Economics, Bertalan Lajos utca 7., Budapest, Hungary, 1111

[b]MTA–BME Research Group for Composite Science and Technology, Műegyetem rakpart 3., Budapest, Hungary, 1111

*Corresponding author

Address: Department of Materials Science and Engineering, Faculty of Mechanical Engineering, Budapest University of Technology and Economics, Bertalan Lajos utca 7., Budapest, Hungary, 1111

Tel: +36 1 463 2386

Fax: +36 1 463 1366

E-mail: orbulov@eik.bme.hu, orbulov@gmail.com

Abstract

Aluminium alloy syntactic foams reinforced with iron hollow spheres were produced by low pressure, liquid phase inert gas infiltration technique. Four Al alloys (Al99.5, AlSi12, AlMgSi1 and AlCu5) and Globomet grade iron hollow spheres were used as matrix and reinforcing material, respectively. The produced composite blocks were characterised according to the ruling standard for compression of cellular materials in order to ensure full comparability. The compressive test results showed plastic yielding and a long, slowly ascending plateau region that ensures large energy absorption capability. The proper selection of the matrix material and the applied heat treatment allows for a wide range of tailoring of the mechanical properties. For design purposes, the full-scale finite element method (FEM) model of the investigated foams was created and tested on Al99.5 matrix foams. The FEM results showed very good agreement with the measured values (typically within 5% in the characteristic properties and within 10% for the whole compression curve).

Keywords: metallic foam, compressive strength, metal matrix composite, hollow sphere, absorbed energy

1. Introduction

Metal matrix syntactic foams (MMSFs) consist of a metallic matrix material and a set of hollow spheres. MMSFs were developed for lightweight structures, requiring high strength and energy absorbing capacity [1]. The matrix material is usually an aluminium alloy (light and low cost), but nowadays high strength iron based matrices are also investigated [2-11]. As filler material, commercially available mixed-oxide ceramic [12-15], metallic [12] or SiC [16, 17] hollow spheres are frequently applied, however Taherishargh et al. have been made efforts for the application of low cost perlite filler as well [18-20].

The professional literature mainly focuses on the production and mechanical properties of MMSFs. For example, Lehmhus and Weise et al investigated the mechanical behaviour of hollow glass microspheres-iron matrix syntactic foams. In particular, the strain-rate sensitivity response at three different strain rate levels was studied by taking into account the influence of type and volume fraction of glass spheres. The materials' behaviour was found to be very similar to that of the metal matrix [2, 6-8]. Castro and Nutt produced steel based MMSFs, filled with ceramic hollow spheres by gravity fed and mechanical pressure infiltration. In the case of gravity fed infiltration the simple compression behaviour of the MMSFs was studied, and a TRIP steel syntactic foam exhibited the highest compression strength and energy absorption capacity [4]. In the case of mechanical pressure infiltration the basic mechanical properties of a ferritic and a pearlitic steel MMSF were studied under compression loading. The pearlitic foam had greater compression strength and energy absorption capacity than the ferritic [5]. The research group of Rabiei studied composite metal foams (CMFs) produced by gravity casting technique. The foam was comprised of steel hollow spheres packed into a random dense arrangement, with the interstitial space infiltrated with a casting aluminium alloy. The composite displayed superior compressive strength (~65 MPa within 10-50% strain range) and energy absorption capacity (~30 MJm^{-3} at 50% strain) [21-24]. Rabiei et al also

published CMFs produced by powder metallurgy. The CMFs were built up from the combination of carbon steel or a 316L grade stainless steel matrix and hollow spheres respectively. The energy absorption at densification for carbon steel samples ranged from 18.9 to 41.7 MJm^{-3} and for the stainless steel sample it was 67.8 MJm^{-3} [3, 22]. Later the effect of loading rate and spheres size were also taken into account: the smaller hollow spheres performed better at each loading rate level up to 8 ms^{-1} [25]. The fatigue properties of Al-steel and steel-steel CMFs under cyclic compression were also described in details [11].

Besides iron based matrices and / or hollow spheres numerous other investigations on the compressive properties of Al based, ceramic hollow sphere filled MMSFs have been published. Balch et al investigated the load partitioning in MMSFs by diffraction techniques and found that the best performance can be achieved if the matrix yield strength and hollow spheres crush strength are equal [26, 27]. Dou and Wu et al investigated the quasi-static and high strain rate response of cenosphere-pure aluminium MMSFs. The foams exhibited distinct strain rate sensitivity, with peak strengths increased from ~45-75 to ~65-120 MPa, and energy absorption capacity increased by ~50-70% [28-30]. Goel et al studied the same material pair of varying densities and cenosphere sizes at different strain rates (0.01…10 s^{-1}). The plateau stress, densification strain, energy absorption and strain rate sensitivity parameter as a function of relative density, strain rate and cenosphere size have been reported [31-33]. Luong et al investigated the quasi-static and high strain rate compressive properties of Al4032 / cenosphere composites. While the matrix did not show any strain rate sensitivity, the composite showed higher strength and energy absorption capability at higher strain rates [34]. Mondal et al performed wide range of materials testing such as classical quasi-static [35], high strain rate [32] or elevated temperature compression [36] tests, wear tests [37, 38] and finite element analyses [39]. Palmer et al studied the mechanical properties of MMSFs incorporating 45 and 270 μm ceramic microspheres in Al1350, Al5083 and Al6061 alloy matrices. The produced foams remained intact at strains up to 50% despite significant fracturing, resulting in high and repeatable strain energies [40]. Kiser et al investigated the mechanical response of a family of ceramic microballoons reinforced Al matrix MMSFs under both uniaxial and constrained die compression loadings. The energy absorption capacity (160±70 MJm^{-3}) found to be extremely high in comparison with values that are typical of metal foams [41]. Beside classical MMSFs (as a base for comparison) [42] Tao et al produced Al particle toughened MMSFs by pressure infiltration. With the introduction of Al particles, the ductility and the compressive strength increased by ~30%. As a result, the specific energy absorption capacity was also increased by ~80% [43]. Subsequently, MMSFs with bimodal ceramic hollow spheres were produced and studied. The MMSFs had ~10% higher porosity, which led to 8% higher densification strain [44]. Zhang and Zhao investigated the mechanical response of four types of Al based MMSF with different sphere sizes and densities under static and dynamic conditions. The plateau strength and the energy absorption of the MMSFs were largely determined by the volume fraction of Al and to a lesser extent by the properties of the ceramic spheres [45]. Although the most common matrix materials are Al and steel, other perspective matrices, such as Mg [46-50], Zn [51, 52] and Ti [53, 54] alloys were also studied.

The modelling of the structure of MMSFs has been also discussed in professional literature. The reconstruction of the structure is often supported by X-ray tomography [55-60] and relies on analytical approaches (for example by Zsoldos et al [61]). Bardella and Genna published papers on the determination of the elastic properties of syntactic foams [62-64]. These articles are based on three phase unit cell models considering the matrix – wall – porosity structure of syntactic foams.

Marur has published a very similar approach [65]. A three phase concentric sphere model was used to estimate the effective elastic constants, and the results were compared to other theories and experimental data. In a subsequent paper Marur took into account the influence of weak interfaces between the inclusion (hollow spheres) and the matrix [66]. Later the applicability of the formulae and the conclusions were also confirmed by numeric methods [67]. Porfiri and Gupta focused on the development of a model to estimate the elastic constants for syntactic foams as function of particle wall thickness, size, and volume fraction. The model can be used to predict the Young's modulus of MMSFs containing microballoons of a wide range of wall thickness and volume fraction [68]. Based on their experimental work [69, 70], Rohatgi and his research group presented a model that can predict peak stress, plateau stress, densification strain, and composite density of hollow ceramic sphere-reinforced MMSFs subjected to unconstrained compression. The results showed good agreement with the experimental data available in literature [71]. Kiser et al gave a prediction for the crush strength of MMSFs in constrained upsetting condition, with an effective strength that depends on the relative wall thickness [41].

According to the above mentioned research contributions the aims of this paper are (i) to give details about the mechanical properties of Al alloy based, Fe hollow sphere reinforced MMSFs; (ii) to describe a full-scale finite element method (FEM) model able to follow the compressive properties of the produced MMSFs.

2. Materials and experimental methods

Four types of MMSF were produced by low pressure inert gas assisted infiltration technique. The applied matrices were Al alloys, their measured chemical compositions are listed in Table 1. For this investigation a PhillipsXL-30 type electron microscope (SEM) equipped with an EDAX Genesis energy dispersive X-ray spectroscopy (EDS) analyser was applied.

Table 1. Chemical composition of the applied matrix materials (only the significant elements are tabulated, measured by EDS)

Matrix	Main components (wt%)						Closest standard equivalent [72]
	Al	Si	Fe	Mg	Cu	Other	
Al99.5	99.5	0.1	0.1	-	-	0.3	Al1050
AlSi12	86.0	12.8	0.1	0.1	-	1.0	A413
AlMgSi1	97.0	1.1	0.5	1.1	-	0.3	Al6082*
AlCu5	95.0	-	-	-	4.5	0.5	Al2011

*Closest alloy, except the Mn content (should be 0.4…1.0 wt%).

Globomet (GM) grade hollow pure Fe spheres were applied as filler material (supplied by Hollomet GmbH, Dresden, Germany [12]). The nominal diameter of the hollow spheres was 1.92±0.07 mm (obtained by measuring 1000 hollow spheres on an Olympus SZX 16 type stereo microscope). Their average wall thickness was 23±0.6 µm, while their density was 0.093 gcm^{-3}. The actual diameter distribution of the spheres followed Gaussian distribution as it is plotted in Fig. 1a. The volume

fraction of the reinforcement was maintained at ~65 vol%, by continuous tapping of the mold [73, 74]. A typical macro photograph and a SEM image about the surface of the hollow spheres are presented in Fig. 1b and Fig. 1c respectively.

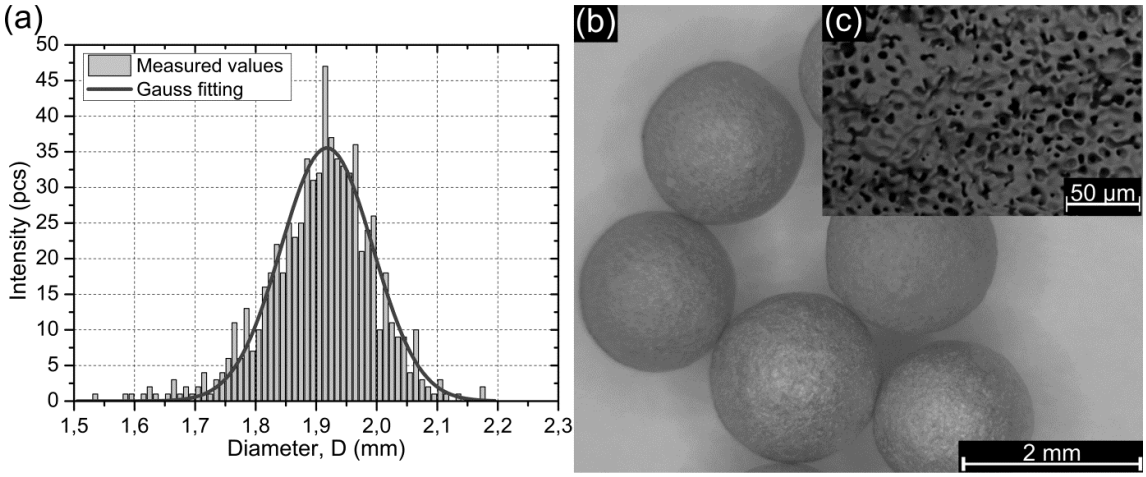

Fig. 1. Diameter distribution of the hollow spheres (a); macro photograph (b) and SEM image (c) about the surface of the hollow spheres

For the infiltration process, a special mold was developed and fabricated (Fig. 2). The mold (#7) was coated by a thin graphite layer (FormKote T-50; Everlube Products, Peachtree City, GA) and filled halfway by the hollow spheres (#6) during continuous tapping in order to achieve ~65% volume fraction [73, 74]. Subsequently, the hollow spheres were fixed in position by a 316L stainless steel net (#5) and placed in a furnace (Lindberg / Blue M) for pre-heating (300°C for 0.5 h). Meanwhile, the matrix material was melted and heated above its melting point by 50°C in a Power-Trak 15-96 induction furnace. In the next step, the molten matrix material (#4) was poured into the mold, on the hollow spheres. Subsequently, the inert gas (Ar) was injected into the system through a pressure reducer and the upper pipe system (#1 and #2) at 400 kPa infiltration pressure. A steel plate (#3) was placed into the way of the gas to break its flow and produce turbulent gas flow. The gas from the space between the hollow spheres was exhausted through the Al_2O_3 mat (#9) stuffed pipe (#8) at the bottom of the mold. After solidification and cooling, the mold was opened by machining (milling) and the MMSF block was removed. The density of the blocks were measured by Archimedes' method, with measured densities of 1.41 gcm^{-3}, 1.42 gcm^{-3}, 1.60 gcm^{-3} and 1.72 gcm^{-3} for the Al99.5, AlSi12, AlMgSi1 and AlCu5 foams, respectively.

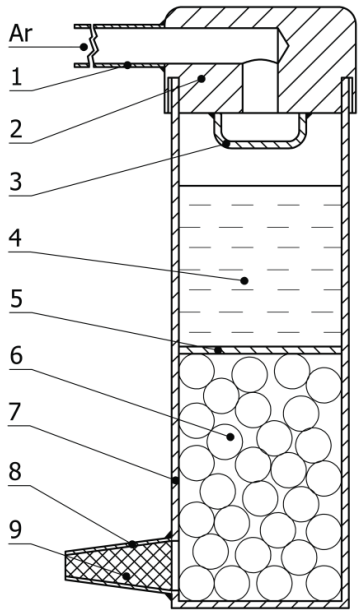

Fig. 2. Schematic sketch of the infiltration system

The produced blocks were solution treated (at 520°C for 1 hour, water cooled). Because of the natural aging (or cold aging) nature of the Cu containing Al alloys, the compression tests were done immediately after the cooling to avoid any effect of natural aging. The AlMgSi1 and AlCu5 specimens were tested in aged condition too (two step T6 treatment (i) homogenisation at 530°C for 1 hour, water cooled and (ii) aging at 170°C for 14 hours, water cooled) Again, the specimens were tested just after the aging step. Six cylindrical specimens for compression tests were machined from each block. Both the diameter (D) and the height (H) of the specimens were 14 mm (H/D=1). The specimens were designated according to their matrix and heat treatment (for example, AlMgSi1-GM-O stands for a specimen with AlMgSi1 matrix and ~65 vol% Globomet grade hollow spheres) in solution treated condition. Two typical optical microscope (Olympus PMG3) images are shown in Fig. 3.

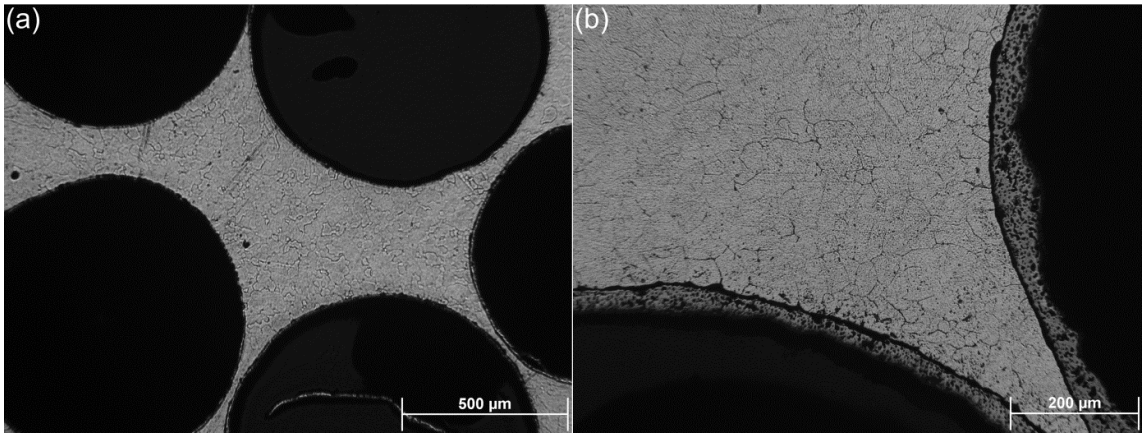

Fig. 3. Typical optical microscope images of Al99.5-GM-O type MMSF at (a) low and (b) higher magnification

In summary 36 compression tests (4 solution treated and + 2 aged matrices, 6 specimens for each combination) were done. The compression tests were performed on a MTS 810 type universal testing machine in a four column tool at room temperature. The surfaces of the tool were hardened to 45 HRC, ground and polished. The specimens and the tool were lubricated with anti-seize material with MoS_2 content. The deformation rate was maintained at 0.01 s^{-1} (quasi-static condition). During the tests the engineering stress – engineering strain curves were registered and processed according to the ruling standard for the compression tests of cellular materials (DIN50134:2008 [75]).

3. Results and Discussion

3.1. Compressive properties

A typical engineering stress – engineering strain curve is shown in Fig. 4 (the initial part of the curve is magnified in the inset figure). Compared to the typical graphs of ceramic hollow sphere reinforced MMSFs, the curve shows some significant difference [76-80]. Most importantly the curve does not have any local maximum, therefore expressed compressive strength cannot be defined. This is caused by the plastic behaviour of the Fe hollow spheres in comparison to the brittle like failure mechanism of the ceramic ones.

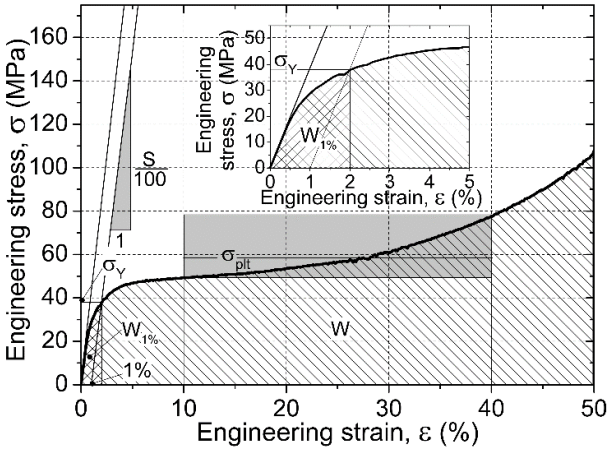

Fig. 4. Typical stress – strain curve of MMSFs showing the characteristic properties

Therefore, instead of the compressive strength the yield strength (σ_Y (MPa)) was determined (similarly to the conventional (0.2%) proof strength, but at 1% strain). At this strain and stress level, macroscopic cracks can be observed on the surface of the specimens in the vicinity of the hollow spheres. According to this, an absorbed energy level required to initialise the fracture process can be

calculated as the integral of the curve up to 1% (the area under the curve up to 1%, $W_{1\%}$ (MJm^{-3})). The slope of the initial part of the graph is the structural stiffness (S (MPa)). The MMSFs showed continuously increasing plateau region, in which case the plateau strength (σ_{plt} (MPa)) can be derived as the average between two distinguished strain ratios (10% and 40% were selected as limits according to the recommendations of the standard [75]). An overall absorbed mechanical energy (W (MJm^{-3})) as the area under the whole curve can also be integrated. The above-mentioned mechanical properties are the characteristic properties of the produced MMSFs and they were monitored in the case of all produced material types. In order to have a better insight to the effect of matrix material the average curves with their scatters are plotted in Fig. 5a.

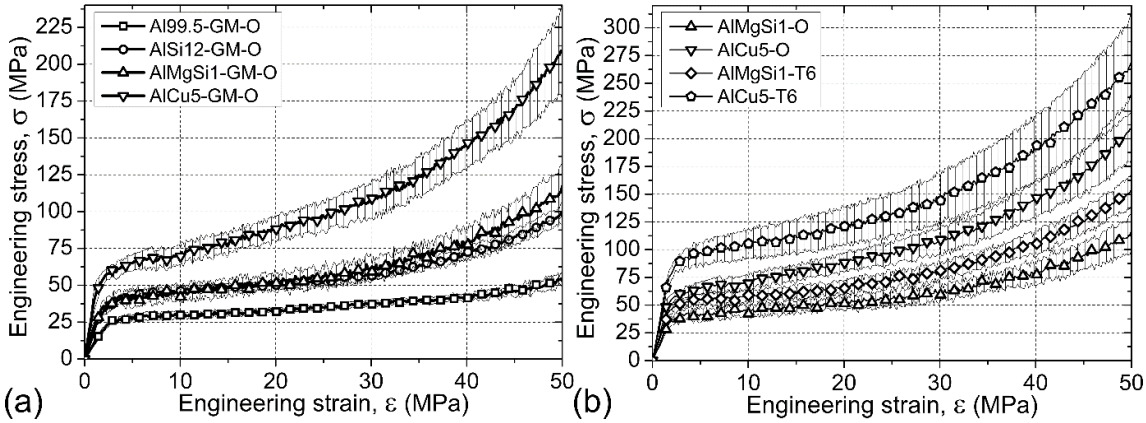

Fig. 5. Effect of the matrix material (a) and the T6 heat treatment (b) on the stress – strain curve

Compared to the unalloyed, Al99.5-GM-O MMSF, the alloyed matrices ensured higher mechanical properties. All the characteristic properties increased significantly due to the solid solution hardening mechanism. The most effective alloying element was the Cu, because of its large diameter difference compared to Al. According to this, the matrix strength had strong influence on σ_Y and σ_{plt}. The difference can be significant, for example, the yield and plateau strength can be increased from ~25 MPa to ~65 MPa and from ~35 MPa to ~75 MPa in the case of solution treated Al99.5 and AlCu5 matrices, respectively. The effect of the matrix material on the $W_{1\%}$ and W absorbed mechanical energy values showed the same trends. The W values varied within wide ranges, from ~1800 MJm^{-3} in the case of Al99.5 matrix up to ~3800 MJm^{-3} in the case of AlCu5 matrix.

The effect of T6 heat treatment is presented in Fig. 5b for AlMgSi1 and AlCu5 matrices. In general, the T6 heat treated specimens showed significantly higher yield strength values, generally by ~30%, than the specimens with solution heat treatment. Compared to the samples with solution treated pure aluminium matrix (~25 MPa) about four times higher yield strength can be achieved by T6 treated AlCu5 matrix (~100 MPa). Moreover, the aged specimens also had higher plateau strength values than the solution heat treated ones, as it is expected. The absorbed energy values ($W_{1\%}$ and W) followed the beneficial effect of the yield and plateau strengths and increased proportionally. It should be noted that, by the hardening effect of the aging process the matrix material has lost some of its ductility and became more brittle and sensitive to cracks. This is associated to the increased

scatter stripe around the average values of the second part of the stress – strain diagrams, showing more probabilistic behaviour than in more ductile cases.

During the compressive tests, different failure mechanisms can be observed in the case of iron sphere reinforced foams. Compared to the MMSFs with ceramic spheres, there was no crack plane and the specimens had plastic deformation in all cases [76, 77]. This observation is supported by the metallographic examinations of compressed specimens, shown in Fig. 6. A high level of plastic deformation of the spheres and matrix material can be observed in the figure. The spheres crushed (black arrow) because of the increasing mechanical pressure, and the matrix tried to follow the deformation of the spheres (white arrow).

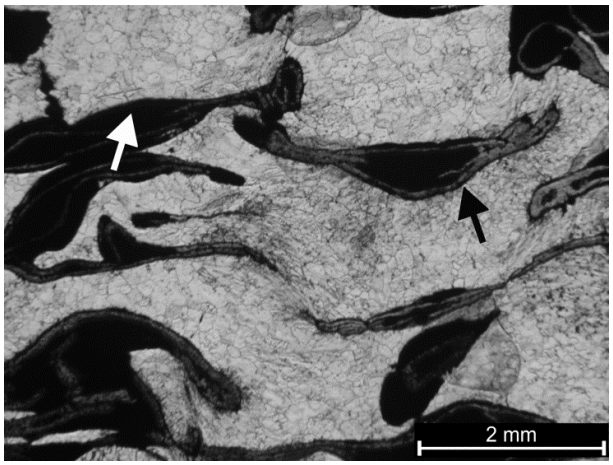

Fig. 6. Polished cross section of a compressed MMSF (AlCu5-GM-O)

In summary, by the application of iron spheres, plastically deformable MMSFs can be produced. Moreover, the mechanical properties can be varied within wide ranges by the proper application of different aluminium alloy matrix materials and heat treatments. The measured properties of the investigated MMSFs are summarised in details in Table 2.

Table 2. The average and scatter values of the investigated characteristic properties

Designation	σ_Y (MPa)	$W_{1\%}$ (MJm^{-3})	S (MPa)	σ_{plt} (MPa)	W (MJm^{-3})
Al99.5-GM-O	26 ± 1	52 ± 5	1090 ± 3	37 ± 2	1772 ± 108
AlSi12-GM-O	35 ± 3	57 ± 7	2369 ± 52	58 ± 3	2870 ± 169
AlMgSi1-GM-O	38 ± 5	71 ± 7	2041 ± 61	63 ± 7	3066 ± 370
AlCu5-GM-O	66 ± 9	102 ± 17	3227 ± 88	74 ± 27	3662 ± 1244
AlMgSi1-GM-T6	51 ± 6	95 ± 9	2730 ± 47	83 ± 8	4038 ± 373
AlCu5-GM-T6	98 ± 9	124 ± 20	3424 ± 75	141 ± 21	5356 ± 1451

3.2. FEM model

The FEM modelling of the MMSFs also has a distinguished importance in the effective and economic design points of view. The full-scale modelling of foams is a hard task because (i) these models are built up from numerous cells, cell walls, junctions, that requires large number of elements and nodes, (ii) the elements often have irregular shapes, (iii) the spaces between the individual hollow spheres are quite small, and therefore the meshing process is complicated. Due to the mentioned problems unit cells are modelled in most cases, however full-scale models can ensure better agreement with the measured values, and the results are more reliable.

In our work, FEM models for unconstrained compression tests were developed, applied and compared to the measured values. The first problem was the proper, probabilistic distribution of the hollow spheres. For this purpose a program, based on a random number generator was developed. The input parameters were: (i) the volume fraction of the hollow spheres, (ii) the diameter distribution of the hollow spheres and (iii) the volume that should be fulfilled. The output was a randomly generated distribution of the hollow spheres in the desired volume and shape (Fig. 7a). The geometric model was built in Creo Parametric 2.0., the meshing was performed in Hypermesh (with the assistance of QI optimised automatic mesh generator). The preferred elements were four node tetrahedrons with average side length of 0.4 mm. The wall thickness of the hollow spheres (modelled by three node triangular shell elements) was set to 23 μm. The meshed model is presented in Fig. 7b. The model was subjected to unconstrained compression in between slowly moving (0.01 s^{-1}) rigid plates. The time step was set to 0.035 s and the test run at ambient temperature. Due to the careful lubrication (and to reduce the running time), the model assumed m=0.2 shear friction (Kudo) coefficient between the specimens and the plates.

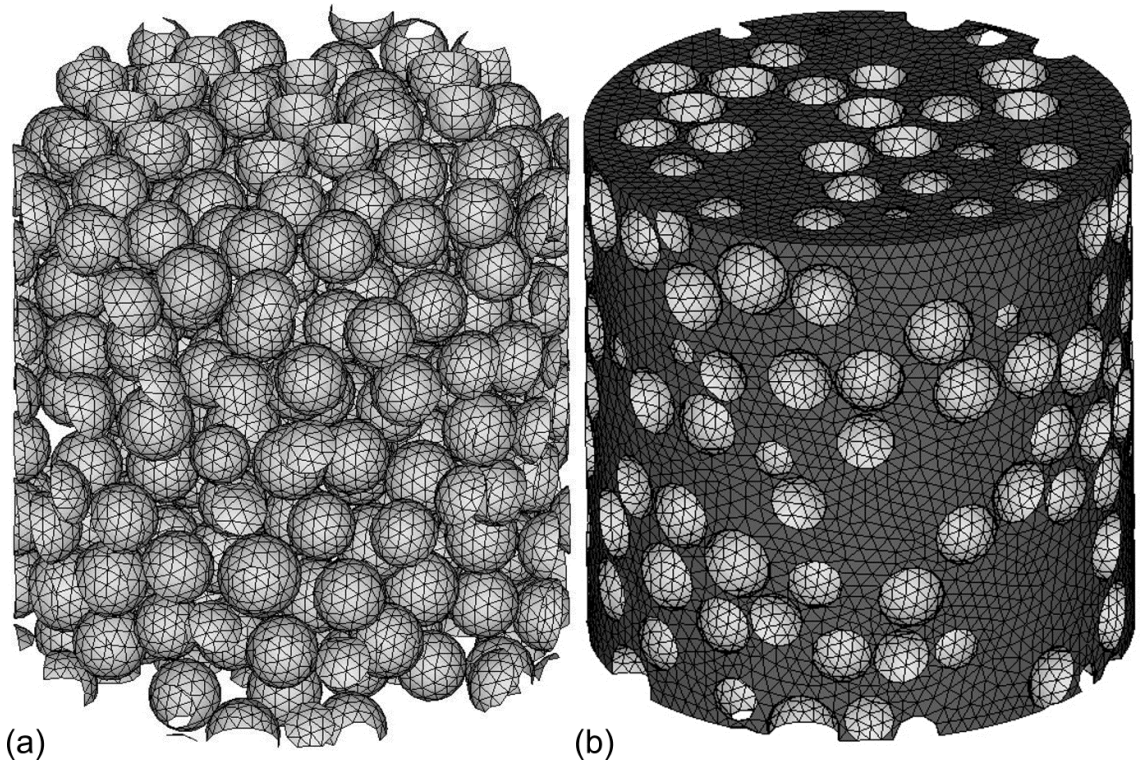

Fig. 7. Distribution of the hollow spheres (a) and the complete, meshed model (b)

The simulation was run on Marc Mentat 2013 environment (with domain decomposition, 8 threads). The model was compressed up to ε=50% and similar to the real measurement the stress – strain curves were calculated. The model was tested on the Al99.5-GM-O specimens and in the case of free compression as the most common loading mode for foams. As input values, the flow curve of the isotropic matrix and filler material are needed. The former was measured by Watts-Ford test [81] (Fig. 8a), while the latter (due to its small contribution to the properties) was assumed to be elastic – ideally plastic with the Young's modulus of 210 GPa and with the flow strength of 300 MPa [82] respectively. The base value of the Young's modulus should be modified due to the relatively large porosity of the sphere walls (Fig. 1b.). For this purpose the equation proposed by Ramakrishnan and Arunachalam was applied [83].

$$E = E_0 \frac{(1-p)^2}{1+\kappa_E} \qquad \text{eq. 1.}$$

Where E is the modified Young's modulus, E_0 is the initial Young's modulus (210 GPa), p is the porosity of the cell wall (estimated as 24% after optical microscopic investigations and image analysis) and κ_E is a constant in terms of the Poisson's ratio (ν_0=0.3) of the fully dense material, defined by eq. 2.

$$\kappa_E = 2 - 3\nu_0 \qquad \text{eq. 2.}$$

The evaluation of the equations above – based on the basic and modified values – results in E=95.9 GPa as input Young's modulus of the spheres for the model. The flow strength of the sphere's wall was also modified, according to eq. 3, suggested by of Liu et al [84].

$$\sigma = K(1-p)^n \sigma_0 \qquad \text{eq. 3.}$$

Where σ is the modified flow strength, σ_0 is the initial flow strength, p is the porosity, K is a material constant (K=0.48 was assumed based on [84]), and n is a material exponent (n=1 is for metals with good plasticity as Cu, Sn, pure Fe and n=1.5 for metals with poor plasticity, like Ti for example). The evaluation of eq. 3 lead to σ=109.4 MPa, in the case of n=1. Because of the already complicated model, perfect bonding and load transfer between the hollow spheres and the matrix material was assumed, as the simplest case. The result of the simulation is shown in Fig. 8b.

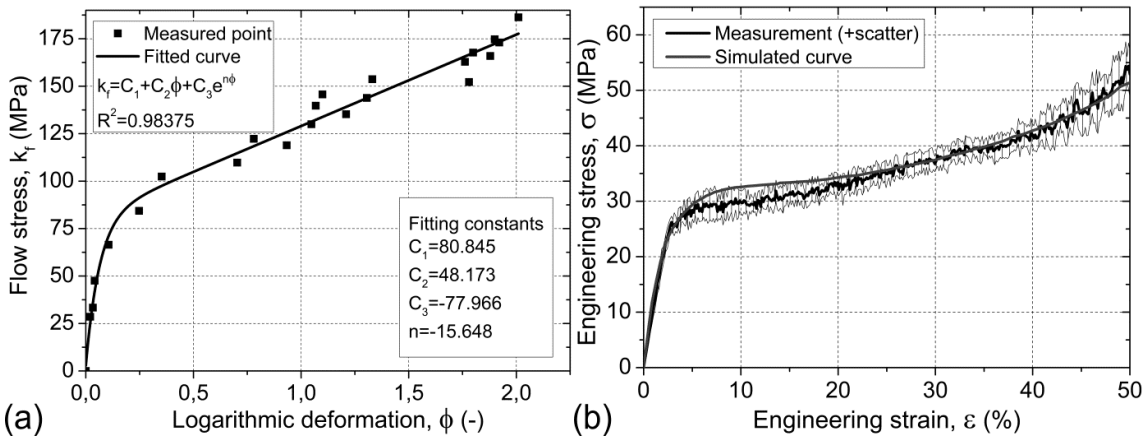

Fig. 8. Flow curve of Al99.5 matrix (a) and the result of the simulation (Al99.5-GM-O)

Fig. 8b. represents excellent agreement between the measured and the simulated curves for Al99.5-GM-O foams. For better comparison, the measured and calculated values of the characteristic properties are listed in Table 3. All the characteristic properties are within a 3% range, except the $W_{1\%}$ energy, that exceeds 6%, but it is still could be considered as a good agreement. As it can be observed in Fig. 8b the calculated curve runs within the scatter band of Al99.5-GM-O specimens, except near to ~10% strain. The largest difference in the stress – strain curve occurs at ε=11%, the difference between the calculated and measured stress is 2.8 MPa (9.3%). In summary, the proposed model is applicable to perform calculations during the design process in virtual environment. However, the model can still be improved by the better estimation of the porosities' effect in the hollow sphere walls and the matrix and by the analysis of the interactions between the spheres and the matrix metal. The model should be also tested and validated on different matrix material that will be reported in a future communication.

Table 3. Comparison of the measured and simulated characteristic properties (Al99.5-GM-O)

	σ_Y (MPa)	$W_{1\%}$ (MJm^{-3})	S (MPa)	σ_{plt} (MPa)	W (MJm^{-3})
Measurement	26 ± 1	52 ± 5	1090 ± 3	37 ± 2	1772 ± 108
Simulation	26.1	55.6	1105.0	37.9	1816.2
Difference (%)	0.38	6.92	1.38	2.43	2.48

Besides the mechanical properties, the deformation mechanism was also followed during the simulation. Again, excellent agreement with the real measurements was found, as it is illustrated in Fig. 9 at the end of the upsetting test (ε=50%).

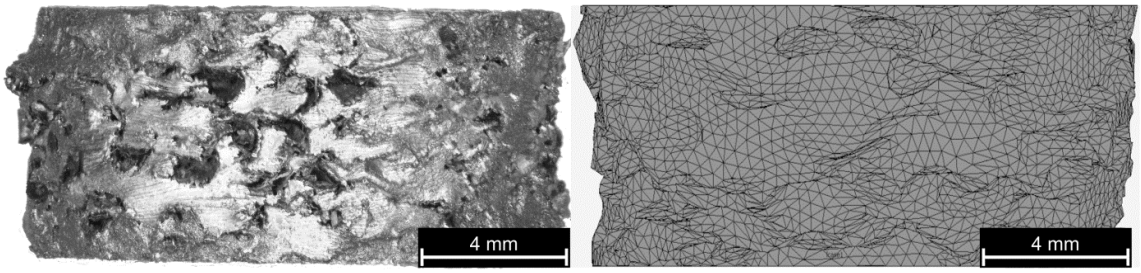

Fig. 9. The deformed shape of Al99.5-GM-O specimen (a) after the test and (b) after the simulation (ε=50% in both cases)

4. Conclusions

From the above detailed investigations and results the following conclusions can be summarized.

- Low pressure, inert gas assisted infiltration technique is suitable method for the production of hollow iron sphere reinforced MMSFs with various Al alloy matrix materials.
- The recorded engineering stress – engineering strain curves showed plastic yielding and long, slowly ascending plateau region that ensures large energy absorption capability; this establishes MMSFs as important candidates for energy absorbing applications.
- The matrix material and the heat treatment have a strong influence on the mechanical properties of the MMSFs; by their proper selection, the characteristic properties can be varied within wide ranges.
- The results of the successfully built, complete and full-scale FEM model gives excellent agreement compared to the measured values for Al99.5-GM-O MMSFs in free compression. The measured values are typically within 5% in the case of characteristic properties and within 10% for the whole curve.

Acknowledgements

This paper was supported by the János Bolyai Research Scholarship of the Hungarian Academy of Sciences.

References

[1] Gupta N, Rohatgi PK. Metal Matrix Syntactic Foams. Lancaster, Pennsylvania, USA: DEStech Publications, Inc.; 2014.
[2] Luong DD, Shunmugasamy VC, Gupta N, Lehmhus D, Weise J, Baumeister J. Quasi-static and high strain rates compressive response of iron and Invar matrix syntactic foams. Mater Des. 2015;66:516-31.
[3] Neville BP, Rabiei A. Composite metal foams processed through powder metallurgy. Mater Des. 2008;29:388-96.
[4] Castro G, Nutt SR. Synthesis of syntactic steel foam using gravity-fed infiltration. Mater Sci Eng A. 2012;553:89-95.

[5] Castro G, Nutt SR. Synthesis of syntactic steel foam using mechanical pressure infiltration. Mater Sci Eng A. 2012;535:274-80.
[6] Peroni L, Scapin M, Avalle M, Weise J, Lehmhus D. Dynamic mechanical behavior of syntactic iron foams with glass microspheres. Mater Sci Eng A. 2012;552:364-75.
[7] Peroni L, Scapin M, Avalle M, Weise J, Lehmhus D, Baumeister J, Busse M. Syntactic Iron Foams - On Deformation Mechanisms and Strain-Rate Dependence of Compressive Properties. Adv Eng Mater. 2012;14:909-18.
[8] Weise J, Salk N, Jehring U, Baumeister J, Lehmhus D, Bayoumi MA. Influence of Powder Size on Production Parameters and Properties of Syntactic Invar Foams Produced by Means of Metal Powder Injection Moulding. Adv Eng Mater. 2013;15:118-22.
[9] Peroni L, Scapin M, Fichera C, Lehmhus D, Weise J, Baumeister J, Avalle M. Investigation of the mechanical behaviour of AISI 316L stainless steel syntactic foams at different strain-rates. Compos Part B. 2014;66:430-42.
[10] Brown JA, Vendra LJ, Rabiei A. Bending Properties of Al-Steel and Steel-Steel Composite Metal Foams. Metall Mater Trans A. 2010;41A:2784-93.
[11] Vendra L, Neville B, Rabiei A. Fatigue in aluminum–steel and steel–steel composite foams. Mater Sci Eng A. 2009;517:146-53.
[12] Hollomet GmbH. <http://www.hollomet.com/home.html> [accessed 18. 12. 14].
[13] Envirospheres Ltd. <http://www.envirospheres.com/products.asp> [accessed 18. 12. 14].
[14] Sphere Services Inc. <http://www.sphereservices.com/> [accessed 18. 12. 14].
[15] Deep Springs Technology. <http://www.teamdst.com/HollowShells.htm> [accessed 18. 12. 14].
[16] Luong DD, Strbik III OM, Hammond VH, Gupta N, Cho K. Development of high performance lightweight aluminum alloy/SiC hollow sphere syntactic foams and compressive characterization at quasi-static and high strain rates. J Alloys and Compounds. 2013;550:412-22.
[17] Rocha Rivero GA, Schultz BF, Ferguson JB, Gupta N, Rohatgi PK. Compressive properties of Al-A206/SiC and Mg-AZ91/SiC syntactic foams. J Mater Res. 2013;28:2426-35.
[18] Taherishargh M, Belova IV, Murch GE, Fiedler T. Low-density expanded perlite–aluminium syntactic foam. Mater Sci Eng A. 2014;604:127-34.
[19] Taherishargh M, Belova IV, Murch GE, Fiedler T. On the mechanical properties of heat-treated expanded perlite–aluminium syntactic foam. Mater Des. 2014;63:375-83.
[20] Taherishargh M, Sulong MA, Belova IV, Murch GE, Fiedler T. On the particle size effect in expanded perlite aluminium syntactic foam. Mater Des. 2015;66:294-303.
[21] Rabiei A, O'Neill AT. A study on processing of a composite metal foam via casting. Mater Sci Eng A. 2005;404:159-64.
[22] Rabiei A, Vendra LJ. A comparison of composite metal foam's properties and other comparable metal foams. Mater Lett. 2009;63:533-6.
[23] Vendra LJ, Rabiei A. A study on aluminum–steel composite metal foam processed by casting. Mater Sci Eng A. 2007;465:59-67.
[24] Vendra L, Rabiei A. Evaluation of modulus of elasticity of composite metal foams by experimental and numerical techniques. Mater Sci Eng A. 2010;527:1784-90.
[25] Rabiei A, Garcia-Avila M. Effect of various parameters on properties of composite steel foams under variety of loading rates. Mater Sci Eng A. 2013;564:539-47.
[26] Balch DK, Dunand DC. Load partitioning in aluminum syntactic foams containing ceramic microspheres. Acta Mater. 2006;54:1501-11.
[27] Balch DK, O'Dwyer JG, Davis GR, Cady CM, Gray Iii GT, Dunand DC. Plasticity and damage in aluminum syntactic foams deformed under dynamic and quasi-static conditions. Mater Sci Eng A. 2005;391:408-17.
[28] Wu GH, Dou ZY, Sun DL, Jiang LT, Ding BS, He BF. Compression behaviors of cenosphere–pure aluminum syntactic foams. Scripta Mater. 2007;56:221-4.
[29] Dou ZY, Jiang LT, Wu GH, Zhang Q, Xiu ZY, Chen GQ. High strain rate compression of cenosphere-pure aluminum syntactic foams. Scripta Mater. 2007;57:945-8.

[30] Zou LC, Zhang Q, Pang BJ, Wu GH, Jiang LT, Su H. Dynamic compressive behavior of aluminum matrix syntactic foam and its multilayer structure. Mater Des. 2013;45:555-60.
[31] Goel MD, Peroni M, Solomos G, Mondal DP, Matsagar VA, Gupta AK, Larcher M, Marburg S. Dynamic compression behavior of cenosphere aluminum alloy syntactic foam. Mater Des. 2012;42:418-23.
[32] Mondal DP, Goel MD, Das S. Effect of strain rate and relative density on compressive deformation behaviour of closed cell aluminum–fly ash composite foam. Mater Des. 2009;30:1268-74.
[33] Goel MD, Mondal DP, Yadav MS, Gupta SK. Effect of strain rate and relative density on compressive deformation behavior of aluminum cenosphere syntactic foam. Mater Sci Eng A. 2014;590:406-15.
[34] Luong DD, Gupta N, Daoud A, Rohatgi PK. High strain rate compressive characterization of aluminum alloy/fly ash cenosphere composites. JOM. 2011;63:53-6.
[35] Mondal DP, Das S, Ramakrishnan N, Uday Bhasker K. Cenosphere filled aluminum syntactic foam made through stir-casting technique. Compos Part A. 2009;40:279-88.
[36] Mondal DP, Jha N, Badkul A, Das S, Khedle R. High temperature compressive deformation behaviour of aluminum syntactic foam. Mater Sci Eng A. 2012;534:521-9.
[37] Mondal DP, Das S, Jha N. Dry sliding wear behaviour of aluminum syntactic foam. Mater Des. 2009;30:2563-8.
[38] Jha N, Badkul A, Mondal DP, Das S, Singh M. Sliding wear behaviour of aluminum syntactic foam: A comparison with Al–10 wt% SiC composites. Tribol Int. 2011;44:220-31.
[39] Mondal DP, Ramakrishnan N, Das S. FEM modeling of the interface and its effect on the elastio-plastic behavior of metal matrix composites. Mater Sci Eng A. 2006;433:286-90.
[40] Palmer RA, Gao K, Doan TM, Green L, Cavallaro G. Pressure infiltrated syntactic foams—Process development and mechanical properties. Mater Sci Eng A. 2007;464:85-92.
[41] Kiser M, He MY, Zok FW. The mechanical response of ceramic microballoon reinforced aluminum matrix composites under compressive loading. Acta Mater. 1999;47:2685-94.
[42] Tao XF, Zhao YY. Compressive failure of Al alloy matrix syntactic foams manufactured by melt infiltration. Mater Sci Eng A. 2012;549:228-32.
[43] Tao XF, Zhao YY. Compressive behavior of Al matrix syntactic foams toughened with Al particles. Scripta Mater. 2009;61:461-4.
[44] Tao XF, Zhang LP, Zhao YY. Al matrix syntactic foam fabricated with bimodal ceramic microspheres. Mater Des. 2009;30:2732-6.
[45] Zhang LP, Zhao YY. Mechanical response of Al matrix syntactic foams produced by pressure infiltration casting. J Compos Mater. 2007;41:2105-17.
[46] Daoud A, Abou El-khair MT, Abdel-Aziz M, Rohatgi P. Fabrication, microstructure and compressive behavior of ZC63 Mg–microballoon foam composites. Compos Sci and Technol. 2007;67:1842-53.
[47] Rohatgi PK, Daoud A, Schultz BF, Puri T. Microstructure and mechanical behavior of die casting AZ91D-Fly ash cenosphere composites. Compos Part A. 2009;40:883-96.
[48] Huang Z, Yu S, Liu J, Zhu X. Microstructure and mechanical properties of in situ Mg_2Si/AZ91D composites through incorporating fly ash cenospheres. Mater Des. 2011;32:4714-9.
[49] Huang Z-Q, Yu S-R, Li M-Q. Microstructures and compressive properties of AZ91D/fly-ash cenospheres composites. Trans of Nonferrous Metals Soc China. 2010;20,458-62.
[50] Luong DD, Gupta N, Rohatgi PK. The high strain rate compressive response of Mg-Al alloy/fly ash cenosphere composites. JOM. 2011;63:48-52.
[51] Daoud A. Effect of strain rate on compressive properties of novel Zn12Al based composite foams containing hybrid pores. Mater Sci Eng A. 2009;525:7-17.
[52] Daoud A. Synthesis and characterization of novel ZnAl22 syntactic foam composites via casting. Mater Sci Eng A. 2008;488:281-95.
[53] Mondal DP, Datta Majumder J, Jha N, Badkul A, Das S, Patel A, Gupta G. Titanium-cenosphere syntactic foam made through powder metallurgy route. Mater Des. 2012;34:82-9.

[54] Xue X-B, Wang L-Q, Wang M-M, LÜ W-J, Zhang D. Manufacturing, compressive behaviour and elastic modulus of Ti matrix syntactic foam fabricated by powder metallurgy. Trans of Nonferrous Metals Soc China. 2012;22:188-92.
[55] Maire E, Colombo P, Adrien J, Babout L, Biasetto L. Characterization of the morphology of cellular ceramics by 3D image processing of X-ray tomography. J European Ceramic Soc. 2007;27:1973-81.
[56] Adrien J, Maire E, Gimenez N, Sauvant-Moynot V. Experimental study of the compression behaviour of syntactic foams by in situ X-ray tomography. Acta Mater. 2007;55:1667-79.
[57] Youssef S, Maire E, Gaertner R. Finite element modelling of the actual structure of cellular materials determined by X-ray tomography. Acta Mater. 2005;53:719-30.
[58] Maire E, Gimenez N, Sauvant-Moynot V, Sautereau H. X-ray tomography and three-dimensional image analysis of epoxy-glass syntactic foams. Phil Trans Royal Soc A. 2006;364:69-88.
[59] Maire E, Fazekas A, Salvo L, Dendievel R, Youssef S, Cloetens P, et al. X-ray tomography applied to the characterization of cellular materials. Related finite element modeling problems. Compos Sci Technol. 2003;63:2431-43.
[60] Kádár C, Maire E, Borbély A, Peix G, Lendvai J, Rajkovits Z. X-ray tomography and finite element simulation of the indentation behavior of metal foams. Mater Sci Eng A. 2004;387–389:321-5.
[61] Kozma I, Zsoldos I, Dorogi G, Papp S. Computer tomography based reconstruction of metal matrix syntactic foams. Per Pol Mech Eng. 2014;58:87-91.
[62] Bardella L, Sfreddo A, Ventura C, Porfiri M, Gupta N. A critical evaluation of micromechanical models for syntactic foams. Mechanics of Mater. 2012;50:53-69.
[63] Bardella L. An extension of the Secant Method for the homogenization of the nonlinear behavior of composite materials. Int J Eng Sci. 2003;41:741-68.
[64] Bardella L, Genna F. On the elastic behavior of syntactic foams. Int J Solids Struct. 2001;38:7235-60.
[65] Marur PR. Effective elastic moduli of syntactic foams. Mater Lett. 2005;59:1954-7.
[66] Marur PR. Influence of imperfect interface on the elastic moduli of syntactic foams. Computat Mater Sci. 2009;46:327-32.
[67] Marur PR. Numerical estimation of effective elastic moduli of syntactic foams. Finite Elements Analysis Des. 2010;46:1001-7.
[68] Porfiri M, Gupta N. Effect of volume fraction and wall thickness on the elastic properties of hollow particle filled composites. Compos Part B. 2009;40:166-73.
[69] Santa Maria JA, Schultz BF, Ferguson JB, Rohatgi PK. Al–Al_2O_3 syntactic foams – Part I: Effect of matrix strength and hollow sphere size on the quasi-static properties of Al-A206/Al_2O_3 syntactic foams. Mater Sci Eng A. 2013;582:415-22.
[70] Santa Maria JA, Schultz BF, Ferguson JB, Guptan N, Rohatgi PK. Effect of hollow sphere size and size distribution on the quasi-static and high strain rate compressive properties of Al-A380-Al_2O_3 syntactic foams. J Mater Sci. 2014;49:1267-78.
[71] Ferguson JB, Santa Maria JA, Schultz BF, Rohatgi PK. Al–Al_2O_3 syntactic foams—Part II: Predicting mechanical properties of metal matrix syntactic foams reinforced with ceramic spheres. Mater Sci Eng A. 2013;582:423-32.
[72] ASM Handbook. Properties and Selection: Nonferrous alloys and Special-Purpose Materials, vol. 2. 2nd printing. ASM International; 1995. p 54.
[73] Jaeger HM, Nagel SR. Physics of the Granular State. Science. 1992;5051:1523-31.
[74] Torquato S, Truskett TM, Debenedetti PG. Is Random Close Packing of Spheres Well Defined? Phys Rev Lett. 2000;84:2064-7.
[75] Testing of metallic materials – compression tests of metallic cellular materials DIN50134 standard; October 2008.
[76] Orbulov IN, Ginsztler J. Compressive characteristics of metal matrix syntactic foams. Compos Part A. 2012;43:553-61.
[77] Orbulov IN. Compressive properties of aluminium matrix syntactic foams. Mater Sci Eng A. 2012;555:52-6.

[78] Orbulov I, Májlinger K. Compressive Properties of Metal Matrix Syntactic Foams in Free and Constrained Compression. JOM. 2014;66:882-91.
[79] Orbulov IN, Májlinger K. Description of the compressive response of metal matrix syntactic foams. Mater Des. 2013;49:1-9.
[80] Májlinger K, Orbulov IN. Characteristic compressive properties of hybrid metal matrix syntactic foams. Mater Sci Eng A. 2014;606:248-56.
[81] Watts AB, Ford H. On the Basic Yield Stress Curve for a Metal. Proc of the Inst of Mech Eng. 1955;169:1141-56.
[82] Carson JM, Hawn JM. Some properties of iron, copper, and selected aluminum alloys including true stress-true strain at reduced temperatures. 1st ed. Ohio: Air Force Materials Laboratory, Air Force System Commands, Wright-Patterson Air Force Base; 1968.
[83] Ramakrishnan N, Arunachalam VS. Effective elastic moduli of porous ceramic materials. J Am Ceramic Soc. 1993;76:2745-52.
[84] Liu P, Fu C, Li T, Shi C. Relationship between tensile strength and porosity for high porosity metals. Sci China Ser E. 1999;42:100-7.

Figure captions

Fig. 1. Diameter distribution of the hollow spheres (a); macro photograph (b) and SEM image (c) about the surface of the hollow spheres

Fig. 2. Schematic sketch of the infiltration system

Fig. 3. Typical optical microscope images of Al99.5-GM-O type MMSF at (a) low and (b) higher magnification

Fig. 4. Typical stress – strain curve of MMSFs showing the characteristic properties

Fig. 5. Effect of the matrix material (a) and the T6 heat treatment (b) on the stress – strain curve

Fig. 6. Polished cross section of a compressed MMSF (AlCu5-GM-O)

Fig. 7. Distribution of the hollow spheres (a) and the complete, meshed model (b)

Fig. 8. Flow curve of Al99.5 matrix (a) and the result of the simulation (Al99.5-GM-O)

Fig. 9. The deformed shape of Al99.5-GM-O specimen (a) after the test and (b) after the simulation (ε=50% in both cases)

Table captions

Table 1. Chemical composition of the applied matrix materials (only the significant elements are tabulated, measured by EDS)

Table 2. The average and scatter values of the investigated characteristic properties

Table 3. Comparison of the measured and simulated characteristic properties (Al99.5-GM-O)

Table-1-R2

Table 1. Chemical composition of the applied matrix materials (only the significant elements are tabulated, measured by EDS)

Matrix	Main components (wt%)						Closest ASM equivalent
	Al	Si	Fe	Mg	Cu	Other	
Al99.5	99.5	0.1	0.1	-	-	0.3	Al1050
AlSi12	86.0	12.8	0.1	0.1	-	1.0	A413
AlMgSi1	97.0	1.1	0.5	1.1	-	0.3	Al6082*
AlCu5	95.0	-	-	-	4.5	0.5	Al2011

*Closest alloy, except the Mn content (should be 0.4…1.0 wt%)

Table-2-R2

Table 2. The average and scatter values of the investigated characteristic properties

Designation	σ_Y (MPa)	$W_{1\%}$ (MJm^{-3})	S (MPa)	σ_{plt} (MPa)	W (MJm^{-3})
Al99.5-GM-O	26 ± 1	52 ± 5	1090 ± 3	37 ± 2	1772 ± 108
AlSi12-GM-O	35 ± 3	57 ± 7	2369 ± 52	58 ± 3	2870 ± 169
AlMgSi1-GM-O	38 ± 5	71 ± 7	2041 ± 61	63 ± 7	3066 ± 370
AlCu5-GM-O	66 ± 9	102 ± 17	3227 ± 88	74 ± 27	3662 ± 1244
AlMgSi1-GM-T6	51 ± 6	95 ± 9	2730 ± 47	83 ± 8	4038 ± 373
AlCu5-GM-T6	98 ± 9	124 ± 20	3424 ± 75	141 ± 21	5356 ± 1451

Table-3-R2

Table 3. Comparison of the measured and simulated characteristic properties (Al99.5-GM-O)

	σ_Y (MPa)	$W_{1\%}$ (MJm^{-3})	S (MPa)	σ_{plt} (MPa)	W (MJm^{-3})
Measurement	26 ± 1	52 ± 5	1090 ± 3	37 ± 2	1772 ± 108
Simulation	26.1	55.6	1105.0	37.9	1816.2
Difference (%)	0.38	6.92	1.38	2.43	2.48

Figure-1

Click here to download high resolution image

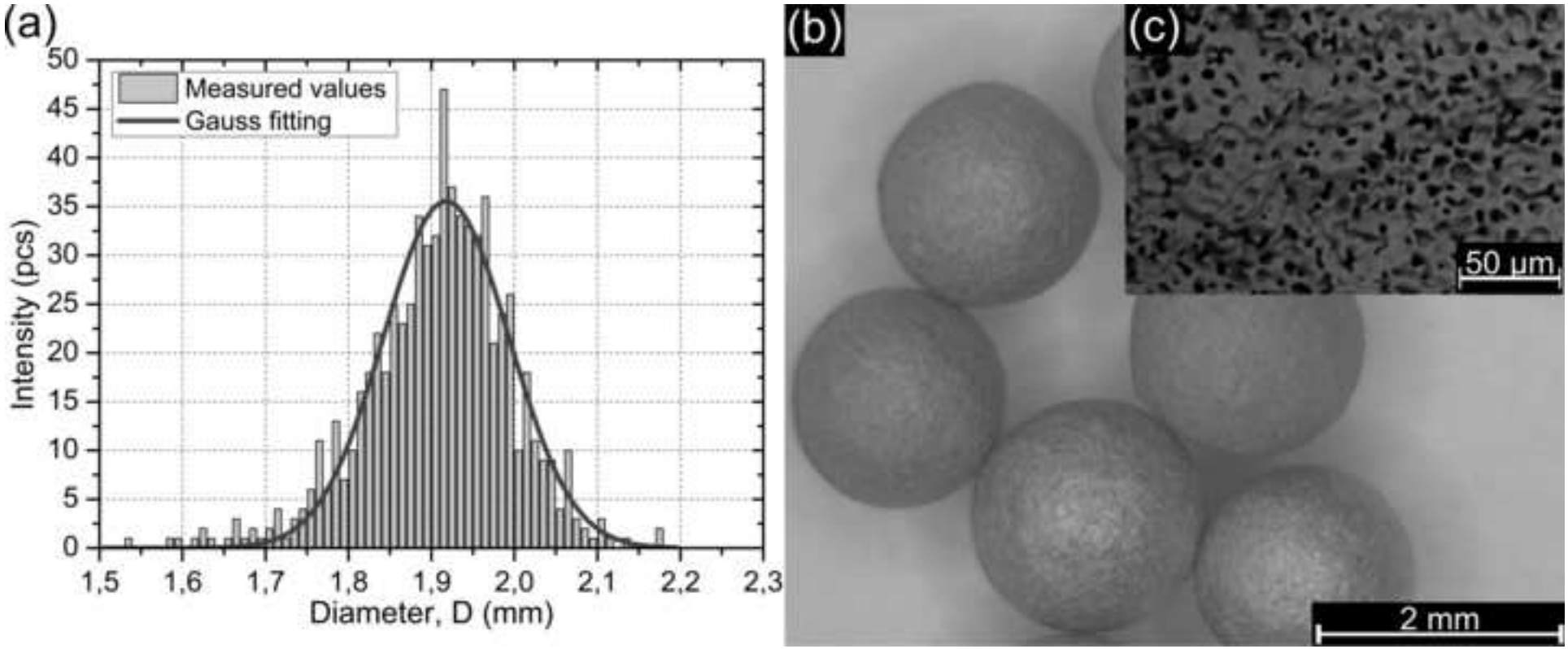

Figure-2

Click here to download high resolution image

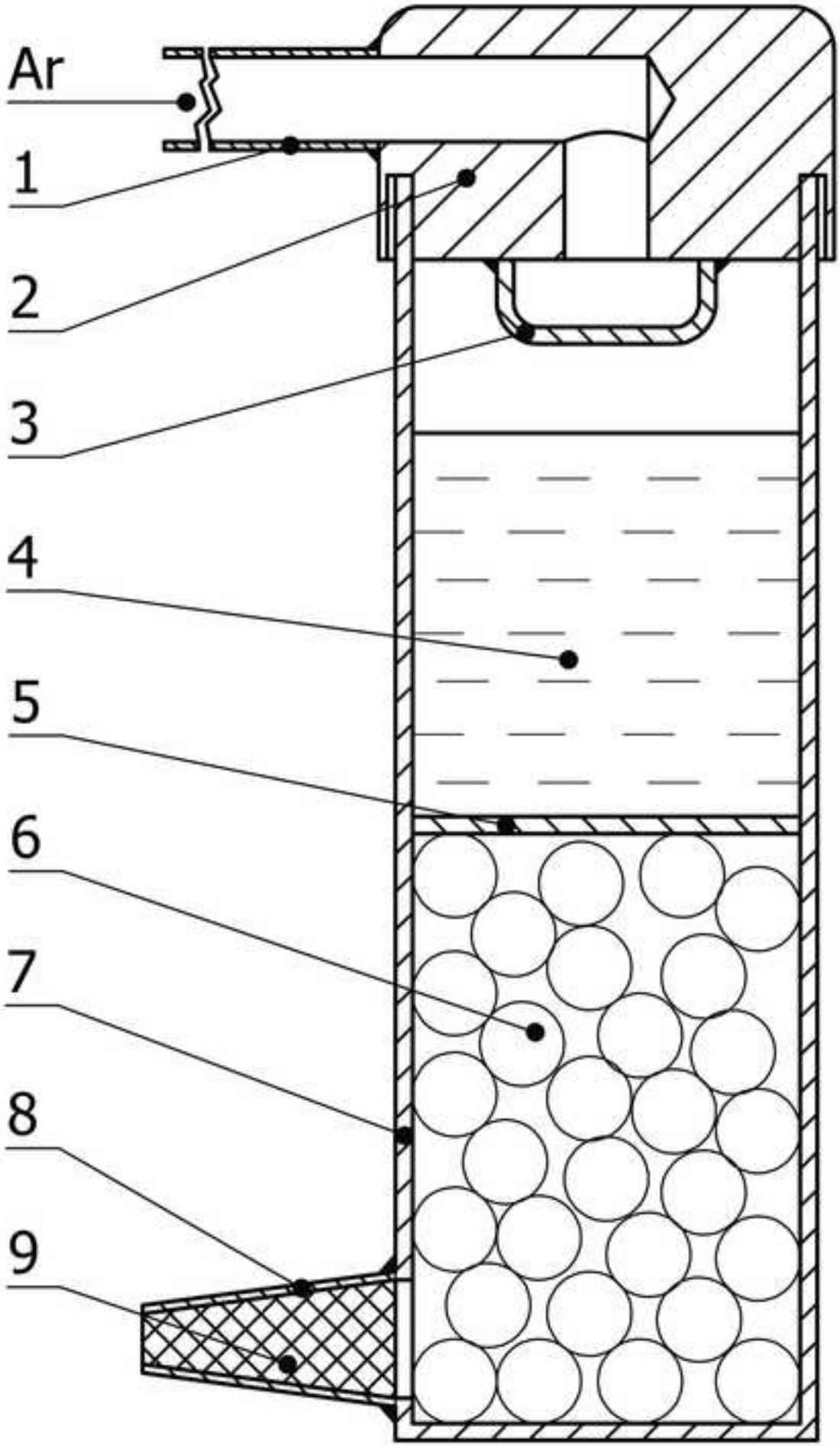

Figure-3
Click here to download high resolution image

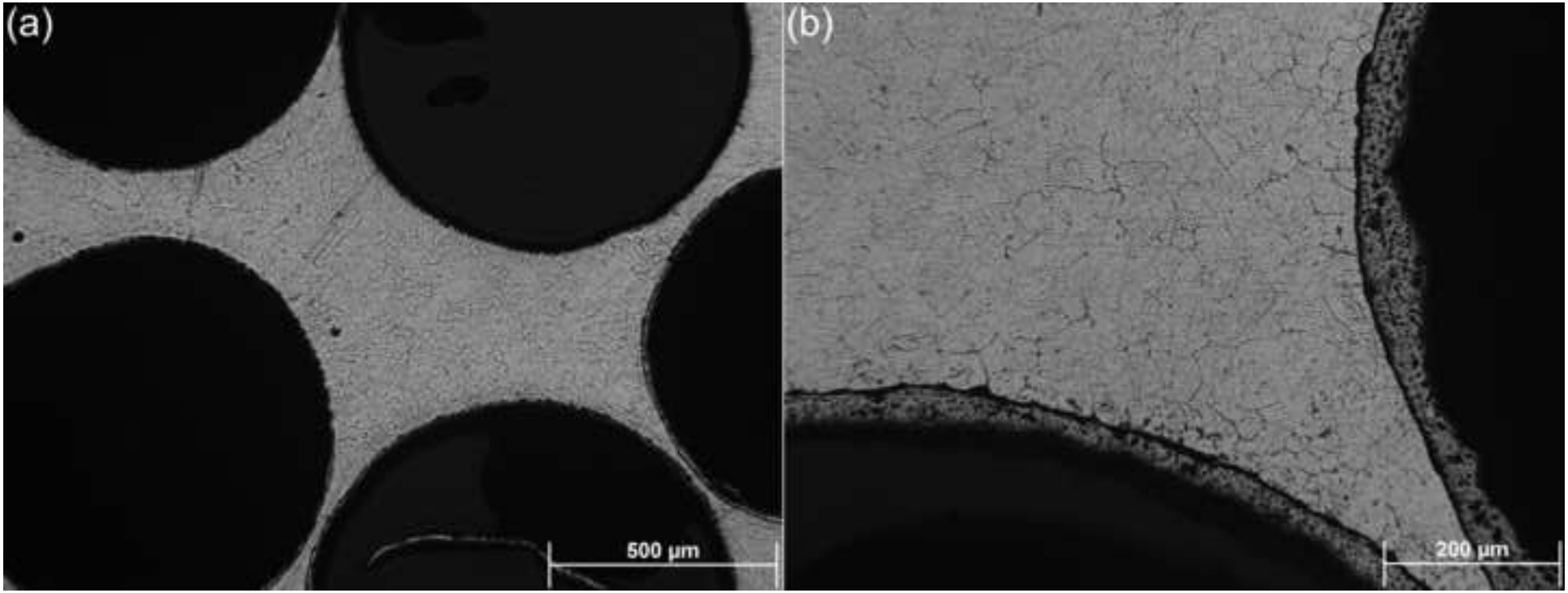

Figure-4-R2

Click here to download high resolution image

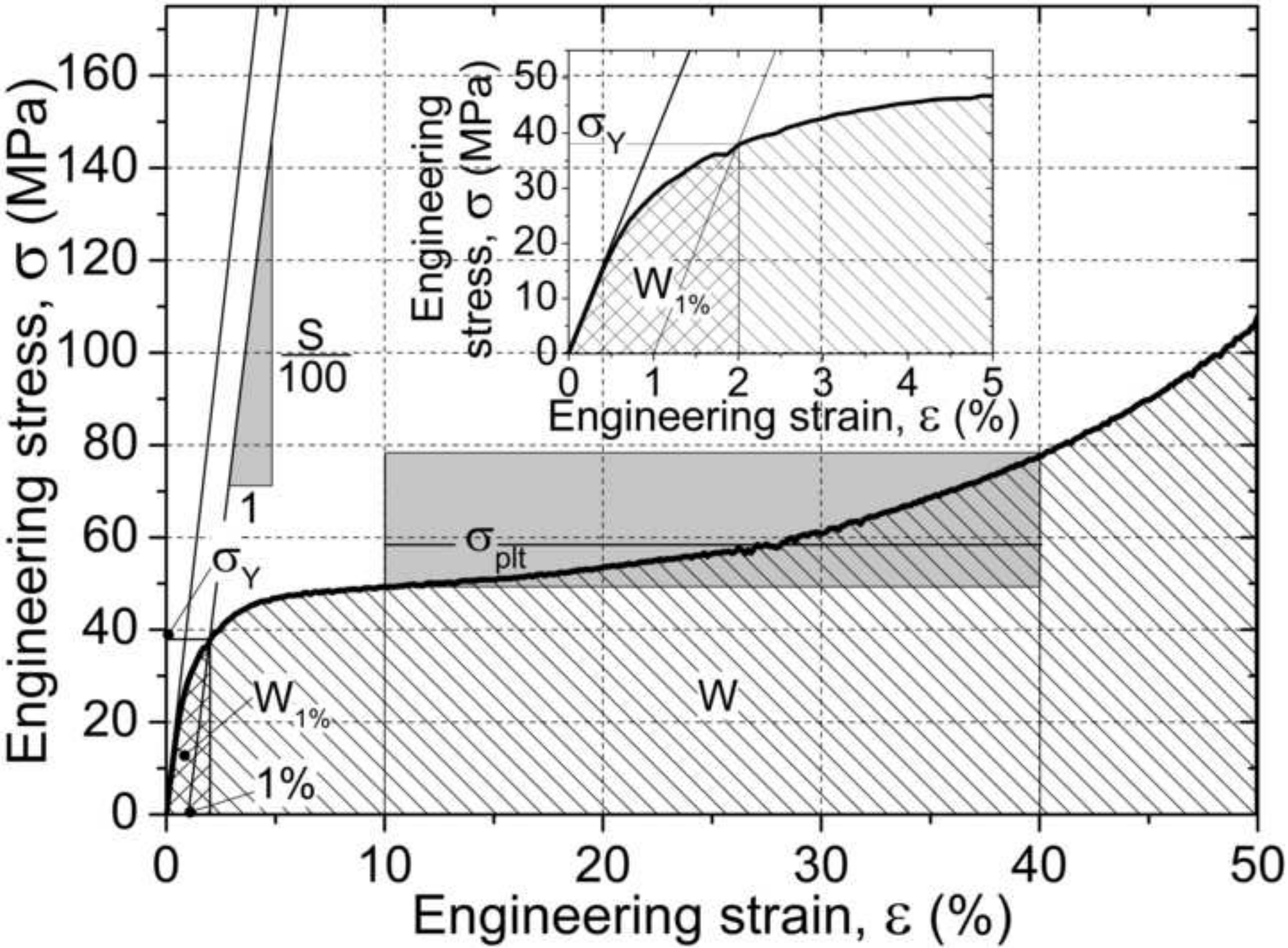

Figure-5-Revised

Click here to download high resolution image

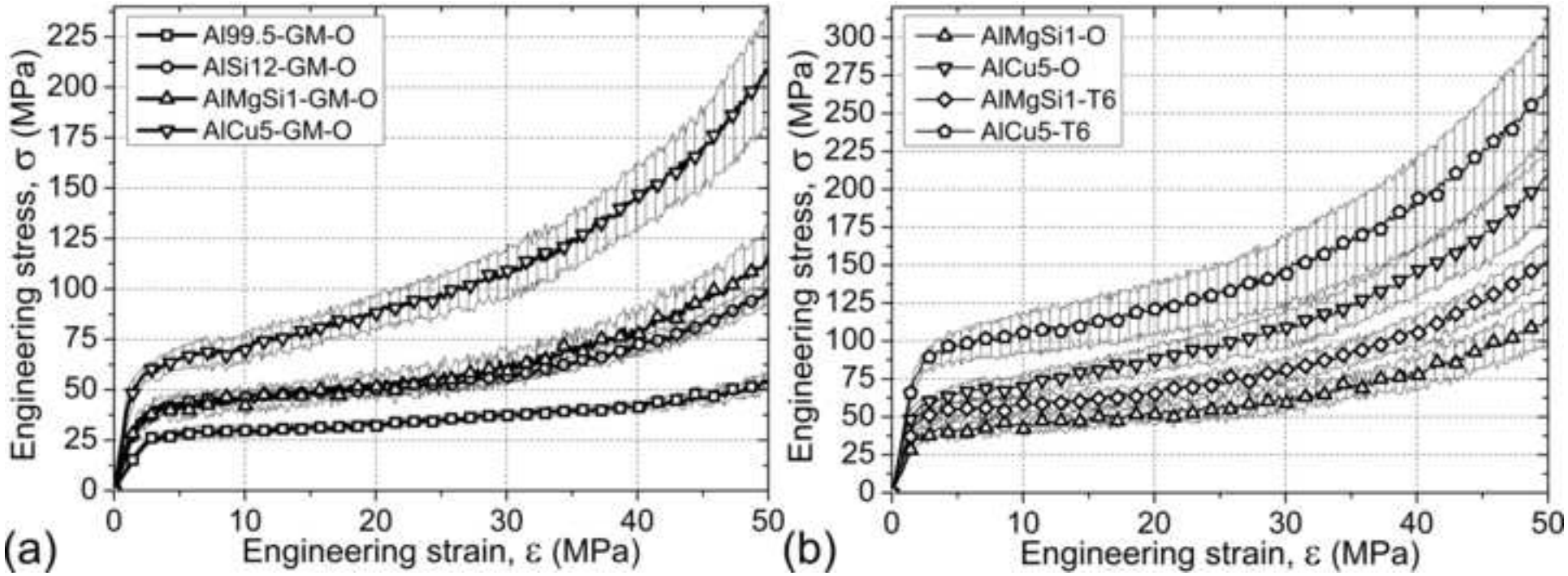

Figure-6

Click here to download high resolution image

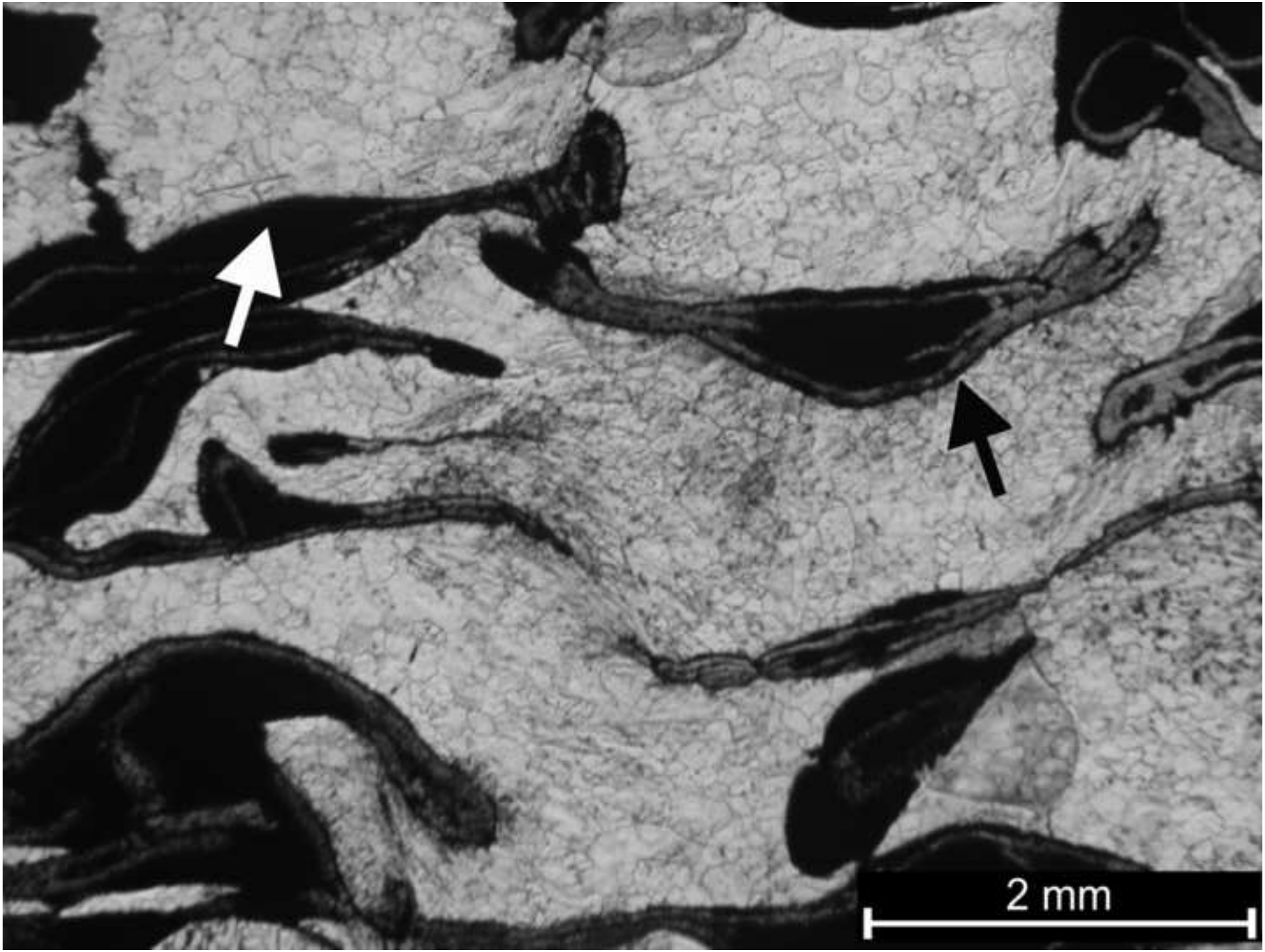

Figure-7

Click here to download high resolution image

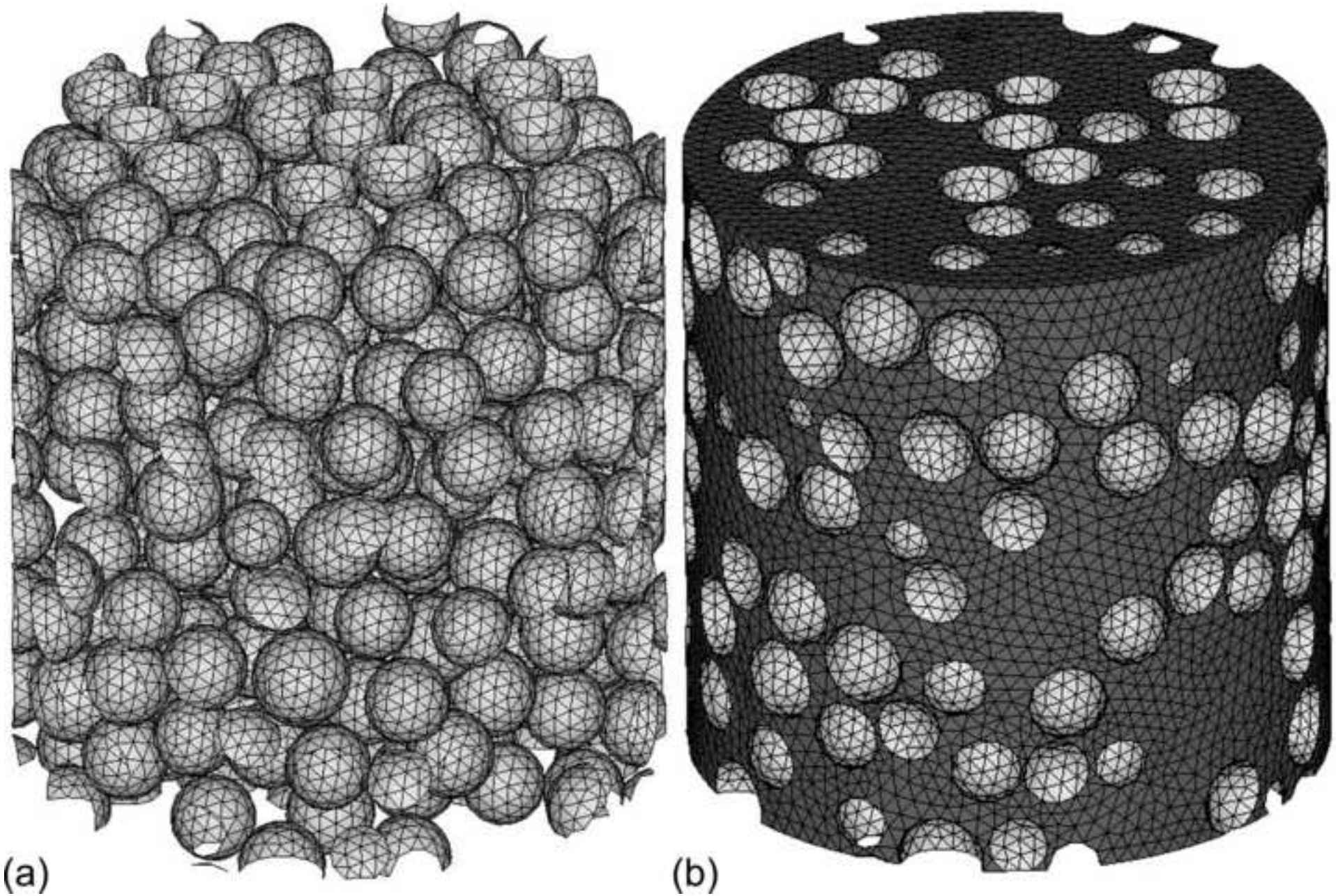

Figure-8

Click here to download high resolution image

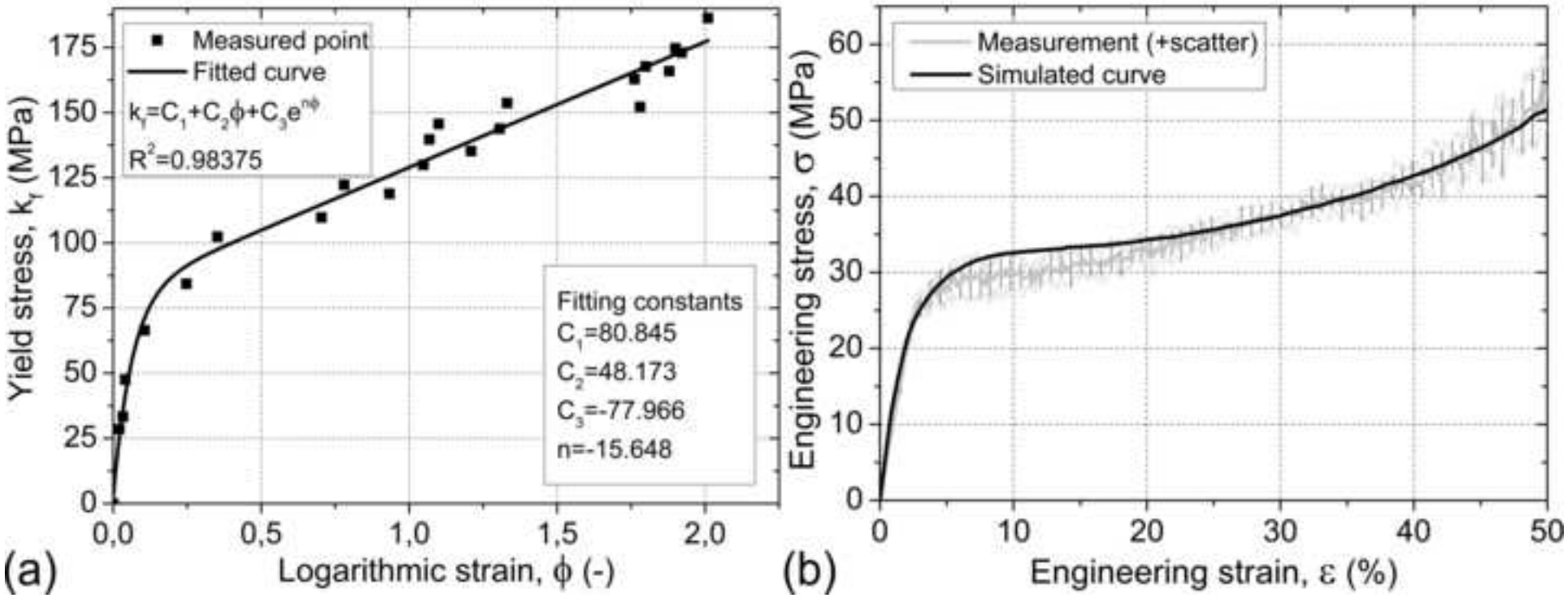

Figure-9

Click here to download high resolution image